

# A Wideband Circularly Polarized Antenna With Metasurface Plane for Biomedical Telemetry

Kai Zhang , Mariella Särestöniemi , Senior Member, IEEE, Sami Myllymäki , Ping Jack Soh , Senior Member, IEEE, Juan Chen , and Sen Yan , Member, IEEE

**Abstract**—This letter presents a metasurface (MS)-based wideband wearable circularly polarized (CP) antenna to communicate with in-body devices. The antenna consists of a crossed dipole, an MS plane and a CP feeding network. The feed network generates a quasi-90° phase delay between each adjacent arm of the crossed dipole. This produces CP radiation and reduces polarization mismatch between the telemetry antenna and the implantable antenna. The MS, consisting of a  $5 \times 5$  unit cell array, functions as a reflector for the crossed dipole to improve forward radiation while maintaining a low-profile structure. This is by designing the unit cells with a near-zero phase reflection over the operating band. To enable conformity with on-body usage, the antenna is designed fully using flexible materials. Textile conductive elements are embedded into a PDMS substrate. It is sized at  $106 \times 106 \times 5 \text{ mm}^3$  ( $1.24\lambda \times 1.24\lambda \times 0.05\lambda$  at 3.5 GHz). Results indicated a  $-10 \text{ dB}$  impedance bandwidth from 2.25 to 6 GHz (90%). The 3 dB axial ratio bandwidth is from 2.9 to 4.95 GHz (52%), with a maximum on-body gain of  $-10.5 \text{ dBi}$ . Finally, the specific absorption rate (SAR) assessment of the antenna indicated values far lower than the limits of the FCC.

**Index Terms**—Biomedical telemetry, circularly polarized antennas, wearable antennas, wideband antennas.

## I. INTRODUCTION

BIOMEDICAL telemetry between implanted and wearable devices has been an important research topic within the context of wireless body area networks (WBANs). Sensing, diagnostics, and communications between them require electronic modules and antennas to receive/transmit signals from/to implantable antennas in the human body from an external on-body antenna [1], [2]. While most antennas introduced to date for this purpose have focused on linearly polarized (LP) antennas, communication with implanted sensors can be more complex

Manuscript received 5 January 2024; accepted 26 February 2024. Date of publication 1 March 2024; date of current version 4 June 2024. This work was supported in part by the National Natural Science Foundation, China Grant 61971340 and Grant 61901351, in part by the Key Research and Development Program of Shaanxi Province, China, under Grant 2022GY-114, and in part by Research Council of Finland Academy Fellowship under Grant 355643. (Corresponding author: Sen Yan.)

Kai Zhang is with the School of Automation and Information Engineering, Xi'an University of Technology, Xi'an 710048, China (e-mail: kai.zhang@xaut.edu.cn).

Mariella Särestöniemi and Ping Jack Soh are with the Centre for Wireless Communications (CWC), University of Oulu, 90570 Oulu, Finland.

Sami Myllymäki is with Microelectronics (MIC) Research Unit, University of Oulu, 90570 Oulu, Finland.

Juan Chen and Sen Yan are with the School of Information and Communications Engineering, Xi'an Jiaotong University, Xi'an 710049, China (e-mail: sen.yan@xjtu.edu.cn).

Digital Object Identifier 10.1109/LAWP.2024.3372197

due to their potentially dynamic location and orientation when they are operating in the body. To overcome this, circular polarization (CP) is effective in minimizing polarization loss, fading and multipath [3], [4].

To enable the CP feature, various design methods have been presented in the literature. In [5], linear polarization feeding structures are used to excite the different current distributions of the polarization rotation artificial magnetic conductor (AMC) to generate a dual polarization in different bands. Another method to generate CP radiation uses an aperture-coupled feed structure, an L-shaped slot and a microstrip line to excite two orthogonal modes with a 90° phase difference based on the characteristic mode theory in [6]. In [7], a novel CP exciting method is presented. An L-shape stub as is introduced as a virtual input port on a double-ring-slot feeding structure to generate a 90° phase delay when the actual port is excited. While such excellent performance is demonstrated in free space, it is known that wearable antenna's reflection and far-field properties can be drastically different when operated on the human body for biotelemetry. Therefore, they must be optimized on phantoms to ensure proper performance.

Besides that, rigid materials employed in these antennas can significantly affect users' comfort levels. In [8], a compact ultra-wideband rigid LP antenna is designed for an implantable system, operating from 3.1 to 10.6 GHz with a transmission loss of  $-14 \text{ dB}$  when implanted at a depth of 10 mm. Another semi-flexible antenna for microwave imaging was proposed in [9]. The rigid monopole antenna is centered on a semi-brick to allow the attachment of the antenna directly to the body. In [10], a bio-matched horn is proposed, consisting of water-filled holes to mimic the frequency-dependent permittivity of the underlying tissues over its entire bandwidth. Evaluation of the antenna's transmission ( $S_{12}$ ) when operated in different rotation angles in both transmit and receive modes indicates that polarization mismatch caused by these rotations deteriorates the link dramatically. To overcome this, a polarization-reconfigurable LP antenna was proposed [11], being able to be switched between 0°, +45°, 90°, and -45° using PIN diodes located on the dipole arms. In [12], a CP receiving antenna is presented for implantable systems. Corner truncations are applied onto a radiator to generate CP waves, whereas a  $4 \times 4$  MS array is used for polarization conversion. However, the antenna is rigid, and its bandwidth is narrow. Moreover, the potential changes in distances between the antenna and human tissue make its performance susceptible to changes. Therefore, decreasing reflection and polarization mismatches are important problems for telemetry antennas.

Metasurfaces (MS) with novel electromagnetic properties have been successfully integrated into wearable antennas to

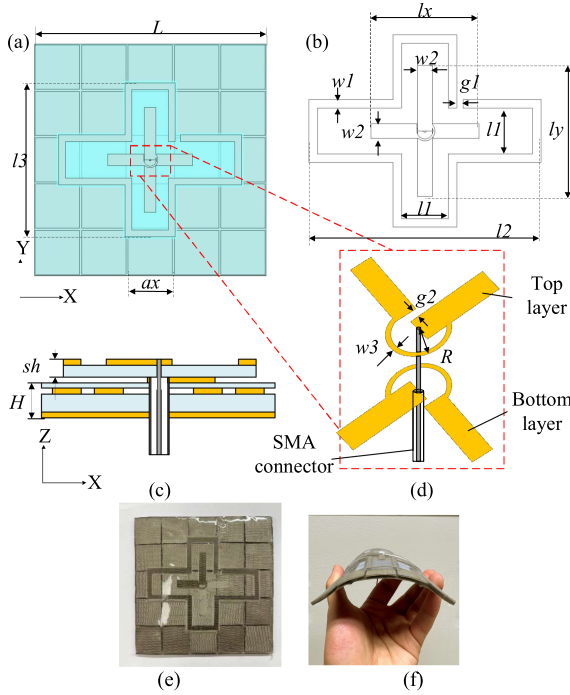


Fig. 1. Antenna model. (a) Top view, (b) feeding structure, (c) side view, (d) feeding structure, (e) prototype, and (f) its flexibility.  $L = 106$ ,  $ax = 20.48$ ,  $w1 = 3.13$ ,  $w2 = 5.48$ ,  $w3 = 0.71$ ,  $lx = 39.28$ ,  $ly = 48.49$ ,  $g1 = 2.30$ ,  $g2 = 0.21$ ,  $sh = 2.00$ ,  $H = 3.50$ ,  $II = 16.96$ ,  $l2 = 84.46$ ,  $l3 = 71.10$ ,  $R = 3.66$  (unit: mm).

improve their performance [13], [14]. One of its most important examples is the application of AMC planes, which can serve as reflectors, extending antenna bandwidth and maintaining a low profile, both in LP and CP antennas [15], [16]. The AMC planes integrated with wearable antennas in [17], [18], and [19] indicated enhanced radiation efficiency and impedance matching. However, a key distinction lies in their radiation direction. They all featured off-body radiation patterns. Besides that, MS-based radiators can be compact wearable antennas designed to resonate at specific frequencies and can be excited using special feeding structures [20], [21], [22]. In improving wearability, the Poly-dimethylsiloxane (PDMS) polymer is widely used in wearable antennas and components due to the flexibility and stability of its electrical properties [19], [20], [21]. This overcomes the shortcomings of textile-based wearable antennas (such as felt and denim), as PDMS is waterproof, transparent, and applicable throughout a wide temperature range ( $-60$  to  $200$  °C). Several PDMS-based wearable antennas have been reported to exhibit excellent performance in free space [23], [24], [25].

This letter presents a highly flexible and wideband CP antenna that radiates towards the human body for biomedical telemetry operating from 2.26 to 6 GHz. Four anticlockwise-rotated arms, each providing a  $90^\circ$  phase delay, are integrated into the antenna to generate a right-handed CP. An AMC plane is used to redirect radiation toward the body to improve forward gain and transmission links while maintaining a low-profile structure besides mechanical flexibility. Simulated and measured results indicated satisfactory performance with the antenna operated on a human phantom with 90% fractional impedance bandwidth and 47.4% fractional AR bandwidth. To the best of our knowledge, this is the first CP antenna with an AMC plane designed and optimized

to be operated in direct contact with the human tissue with such levels of bandwidth, AR bandwidth and gain for this application.

## II. ANTENNA DESIGN AND PRINCIPLES

The proposed antenna is shown in Fig. 1. The flexible PDMS substrate is 2 mm and 3.5 mm thick, with a relative permittivity of 2.75 and a loss tangent of 0.002. Conductive elements of this antenna are formed using conductive textiles embedded into the substrate. This textile is 0.017 mm thick with an effective conductivity of  $1.18 \times 10^5$  S/m. An AMC plane consisting of an array of  $5 \times 5$  patches works as a reflector, whereas a crossed dipole functions as the CP radiator. An unconnected ring surrounding the crossed arms is used for impedance matching. The antenna prototype and its flexibility are shown in Fig. 1(e) and (f), and all the parameters of the antenna are listed in the caption of Fig. 1.

Throughout the design, a phantom is used to optimize the antenna. This phantom consists of three layers of tissues, i.e., a 2 mm thickness of skin layer, a 15 mm thickness of a fat layer, and a 15 mm thickness of muscle layer. The overall dimension of the phantom block is  $200 \times 200 \times 32$  mm<sup>3</sup>, and their electrical parameters are obtained from the CST material library.

### A. Feeding Structure

The exploded view of the feeding structure is shown in Fig. 1(b). The topmost layer consists of a pair of crossed dipoles and a strip loop with a slot. The core of the coaxial cable is connected to one of the top arms, as shown in Fig. 1(d). A meandered line with a  $90^\circ$  phase delay connects this arm with the other arm on the same layer. On the bottom layer of this PDMS substrate, two additional orthogonal arms, symmetrically positioned to the arms on the top layer, are embedded into the substrate. The outer conductor of the coaxial cable is connected to one of the arms on the bottom layer, as in Fig. 1(d), whereas a  $90^\circ$  microstrip line is used to connect the two bottom arms. This generates a phase difference of a quarter wavelength between the adjacent orthogonal arms in an anti-clockwise direction, thus exciting a right-hand CP characteristic.

### B. Metasurface Design

Considering its application in telemetry, the front-to-back ratio (FBR) is important to ensure satisfactory focus of signal going through/ coming from the human body. At the same time, a low-profile structure is important to ensure users' comfort. To enable both features, an AMC plane is designed and integrated into the antenna as a magnetic conductor. The metasurface consists of an array of AMC unit cells made using conductive textiles, as shown in Fig. 1(a). The side view of the antenna is shown in Fig. 1(c), with the textile marked in yellow and PDMS in blue. The fabrication process of the proposed antenna is illustrated in [25]. The unit cell is simulated and optimized in CST with a Floquet port placed above it and a periodic structure boundary. The reference plane of the port is set on the interface between the unit cell and the free space. The simulated reflection phase of this independent unit cell is presented in Fig. 2(a). The reflection phase at the reference surface is presented, and the unit cell operates within the range of  $\pm 90^\circ$  from 3.15 to 5 GHz.

Moreover, it is evident from Fig. 2(b) that the AMC plane enables wideband matching. This can be observed when assessing the performance of the antenna with and without the AMC

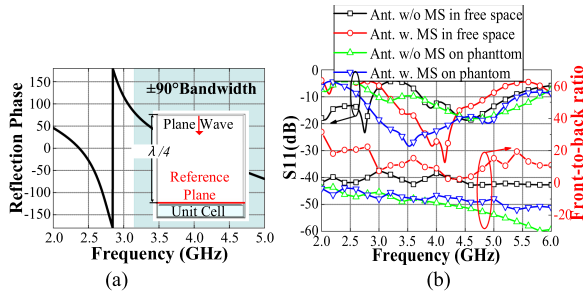


Fig. 2. Performances of the antenna. (a) Reflection phase of a unit cell, (b)  $S_{11}$ , and FBR ( $E_{+z}$ )/( $E_{-z}$ ) results. w/o = without, w. = with.

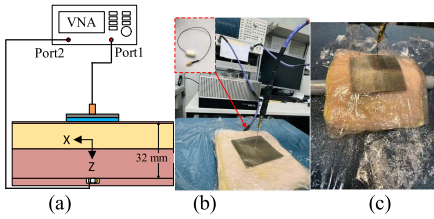


Fig. 3. (a)  $S_{12}$  measurement setup. (b) Wireless link measurement between the capsule and proposed antenna. (c) Antenna evaluation on phantom.

plane. When operating on the phantom, both antennas (with and without AMC plane) operated in a wide bandwidth due to their contact with the lossy phantom. Despite being wider in bandwidth, the FBR ( $E_{+z}$ )/( $E_{-z}$ ) of the crossed dipole without the AMC plane is worse when operating on the phantom, as shown in Fig. 2(b), with positive values indicating a main beam direction towards  $+z$ , and vice versa. While the AMC plane increased the FBR when evaluated in free space, reflection coming from the phantom is mitigated to some extent when the antenna is operating on it. Moreover, the contribution of the AMC plane in mitigating reflections also becomes more evident with increasing frequency.

### III. RESULTS AND DISCUSSION

To experimentally evaluate the antenna similarly to simulations, the PDMS antenna is placed on a fabricated four-layered semi-solid phantom, as shown in Fig. 3. It consists of a 2 mm-thick skin, 15 mm-thick fat, 15 mm-thick muscle, and 5 mm-thick (bottom) muscle cover, as shown in Fig. 3(a). This semi-solid phantom mimics the intestinal tissue [26]. SPEAG's dielectric assessment kit (DAK) is used to measure the electrical properties of each layer [27] when connected to a vector networks analyzer (VNA) 8720ES.

#### A. S-Parameter Performance

For wireless link assessments, an implantable capsule antenna illustrated in Fig. 3(b) is used as a reference antenna. It is placed inside the tissue block and parallel to the center of the proposed antenna [28]. The capsule antenna is linearly polarized, featuring an omnidirectional radiation pattern with a maximum gain of  $-12.6$  dBi in a phantom. Ports 1 and 2 are shown in Fig. 3(a). To evaluate the contribution of the proposed CP characteristic on the wireless link, the capsule antenna was evaluated when rotated around the z-axis at three angles ( $0^\circ$ ,  $45^\circ$ , and  $90^\circ$ ).

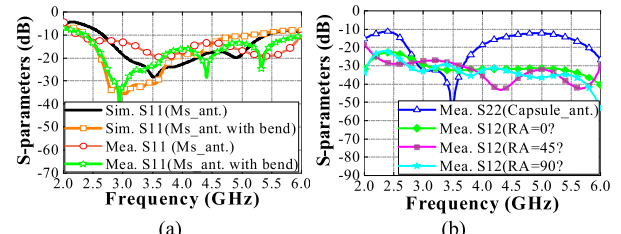


Fig. 4. S-parameters curves of the antenna on the phantom. (a) Simulation and measurement results and (b) measurement results of the wireless link in different cases. Ms\_ant. = metasurface antenna, and RA = rotation angle.

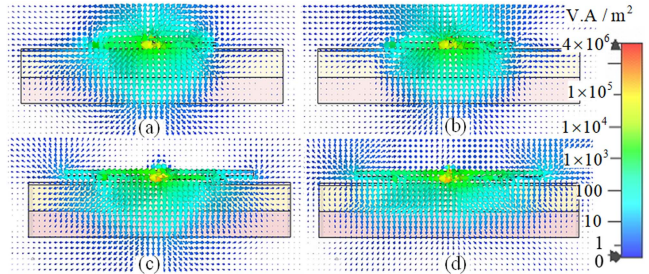


Fig. 5. Power flow distribution (a) without AMC at 3 GHz, (b) without AMC at 4 GHz, (c) with AMC at 3 GHz, and (d) with AMC at 4 GHz.

Results presented in Fig. 4 indicated that the  $S_{11}$  of the proposed antenna operated on phantom from 2.66 to 5.41 GHz in simulations, and from 2.25 to 6 GHz in measurements. At the same, the performance of the antenna with a bend is also shown in Figs. 4(a) and 5(b). The  $S_{11}$  curves of the bent antenna are consistent, showing stable reflection performance and excellent flexibility when applied on an uneven test surface. Measurements indicated wider bandwidth due to the loss and high relative permittivity of the phantom. Differences observed between simulations and measurements can be explained by several factors. Firstly, the uneven phantom thickness fabricated created some variation in the practical test environment relative to simulations. Secondly, parameters of the human body change with frequency slightly, whereas this is rather consistent when extrapolated in the simulator. Finally, slight deviations in the fabricated antenna dimensions affected its reflection coefficient in practice.

Note also that the measured reflection coefficient of the capsule antenna is indicated by the blue  $S_{22}$  line. From the experimental  $S_{21}$  curves, the maximum transmission loss is 22.5 dB at 2.5 GHz. This indicates a consistent link performance within the working band. In Fig. 4(b), the link performance of this antenna is compared against an LP on-body antenna from [2]. This previous antenna is set as an LP receiver, whereas the capsule antenna from Fig. 3(b) is set as an LP transmitter antenna. The average values of  $S_{12}$  over the operating band with different rotation angles are calculated, and the results indicate that the link performance of the CP antenna is better than LP antenna at different rotation angles. The result attenuates greatly when the receiver antenna is LP, and the capsule antenna is rotated by  $90^\circ$ . The wireless link attenuation due to the polarization mismatch is reduced when the capsule antenna is rotating at random orientations inside the body relative to the proposed CP antenna.

TABLE I  
COMPARISON OF THE PROPOSED ANTENNA WITH OTHER RELEVANT LITERATURE

Ref.	Freq. (GHz)	BW	CP/LP	3dB AR BW with phantom	Gain with phantom(dBi)	Flexible	WL /implant depth(mm)	Distance from tissue (mm)
[2]	3.1-10.6	108%	LP	/	/	Rigid	-14dB/10	0
[3]	2.45	5.7%	CP	3.7%	/	Rigid	-28dB/2	40
[9]	0.8-1.2	40%	LP	/	/	Semi	-46dB/100	25
[10]	1.4-8.5	69%	LP	/	/	Rigid	-30dB/35	0
[11]	2.2-3.1	34%	LP	/	/	Rigid	-40dB/5	300
This work	2.25-6	90%	CP	47.4%	-10.5	Flexible	-22.5dB/32	0

BW: bandwidth, CP/LP: circular/ linear polarization, AR: axial ratio, WL: wireless link.

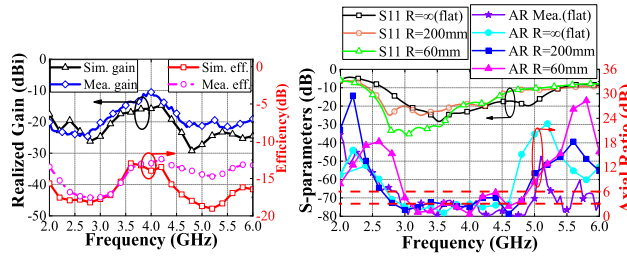


Fig. 6. Far-field performances of the antenna on the phantom. (a) Gain ( $+z$ -direction) and efficiency (flat) and (b) axial ratio.

### B. Near Field Performance

Fig. 5 illustrates the direction of the wave and power flow in the phantom with and without the AMC plane at two main frequencies. The energy in each layer of the phantom has different intensities and distributions depending on each layer's permittivity and loss factor. Compared to the radiator without the AMC plane, the back radiation is almost fully reflected by the AMC plane, indicating its contribution to the antenna performance.

### C. Far-Field Performance

The on-phantom radiation performance of the antenna is then evaluated using a commercial near-field measurement system from SATIMO. The measured gain and efficiency are compared with simulations in Fig. 6(a), indicating satisfactory agreements. The measured peak realized gain is  $-10.5$  dBi at 4 GHz due to absorption by the tissue. Besides that, the measured AR in the  $+z$ -direction toward the phantom is presented in Fig. 6(b), indicating the AR band from 2.9 to 4.7 GHz with a 47.4% relative bandwidth. Small ripples are observed in measurements due to the nonperfect alignment of the antenna with the horizontal plane, besides the slight nonuniform thicknesses of the fabricated phantom. The normalized far-field patterns in the  $+z$ -direction are illustrated in Fig. 7. Simulated gains in the  $+z$ -direction are  $-24.6$  dBi at 3 GHz and  $-15.7$  dBi at 4 GHz, whereas measured gains are  $-20.2$  dBi and  $-10.5$  dBi at the same frequencies, respectively. Fig. 6(b) depicts the antenna's on-phantom performance with different curvature radius,  $R$ . Results indicate that as the radius of curvature decreases, the  $S_{11}$  curve exhibits some degradation. However, it is important to note that the antenna still operated within the target frequency band with  $S_{11} < -10$  dB, ensuring its functionality. A slight deterioration is observed for AR as the bending curvature increases. Nevertheless, the overall AR performance remains below 6 dB, which meets most practical requirements.

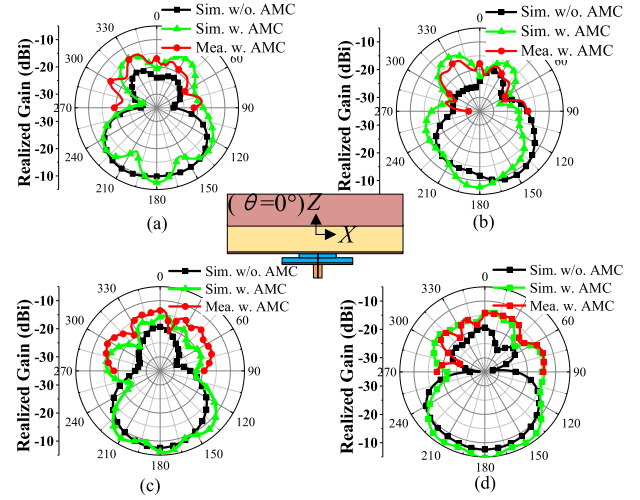


Fig. 7. Far-field pattern in simulations and measurements. (a) 3 GHz  $\phi = 0^\circ$ . (b) 3 GHz  $\phi = 90^\circ$ . (c) 4 GHz  $\phi = 0^\circ$ . (d) 4 GHz  $\phi = 90^\circ$ .

### D. SAR Evaluations

To validate its potential for on-body applications, the specific absorption rate (SAR) of the proposed antenna is evaluated. Based on FCC standards, SAR levels are regulated to be below 1.6 W/kg when averaged over 10 g of actual tissue. The peak averaged SAR values are 0.97 W/kg and 0.51 W/kg at 3 and 4 GHz, respectively, when evaluated with an input power of 0.1 W. Both values are much lower than the FCC requirements.

## IV. CONCLUSION

In this letter, a flexible wideband CP MS-based antenna is proposed for biomedical telemetry with an implanted capsule. The antenna consists of a crossed dipole, an AMC plane, and a feeding structure. A ring-shaped feeding circuit with four arms excites these antenna elements and generates CP radiation. The antenna is made using flexible materials, with conductive textiles as its conductive parts and is embedded in a PDMS substrate. The overall size of the flexible antenna is  $106 \times 106 \times 5$  mm $^3$  at 3.5 GHz ( $1.24\lambda \times 1.24\lambda \times 0.05\lambda$ ), featuring a 90% impedance bandwidth (from 2.25 to 6 GHz with a 3 dB AR bandwidth of 47.4% (from 2.9 to 4.7 GHz)). The maximum radiation gain towards the body is  $-10.5$  dBi. This is also evident from Table I that the proposed antenna's performance, when benchmarked against recent state-of-the-art designs, offers unique innovativeness and improvements.

## REFERENCES

- [1] H. M. E. Misilmani, T. Naous, S. K. A. Khatib, and K. Y. Kabalan, "A survey on antenna designs for breast cancer detection using microwave imaging," *IEEE Access*, vol. 8, pp. 102570–102594, 2020.
- [2] M. Särestöniemi, A. Taparugssanagorn, J. Wisamongkol, M. Hämäläinen, and J. Iinatti, "Comprehensive analysis of wireless capsule endoscopy radio channel characteristics using anatomically realistic gastrointestinal simulation model," *IEEE Access*, vol. 11, pp. 35649–35669, 2023.
- [3] M. Farahani, M. Akbari, M. Nedil, A.-R. Sebak, and T. A. Denidni, "Millimeter-wave dual left/right-hand circularly polarized beamforming network," *IEEE Trans. Antennas Propag.*, vol. 68, no. 8, pp. 6118–6127, Aug. 2020.
- [4] A. Altaf, Y. Yang, K.-Y. Lee, and K. C. Hwang, "Circularly polarized spidron fractal dielectric resonator antenna," *IEEE Antennas Wireless Propag. Lett.*, vol. 14, pp. 1806–1809, 2015.
- [5] H. Yang, X. Liu, Y. Fan, and L. Xiong, "Dual-band textile antenna with dual circular polarizations using polarization rotation AMC for off-body communications," *IEEE Trans. Antennas Propag.*, vol. 70, no. 6, pp. 4189–4199, Jun. 2022.
- [6] Z. Zhang, Y. Cheng, H. Luo, and F. Chen, "Low-profile wideband circular polarization metasurface antenna with characteristic mode analysis and mode suppression," *IEEE Antennas Wireless Propag. Lett.*, vol. 22, no. 4, pp. 898–902, Apr. 2023.
- [7] Y. Zhang, Y. Zhang, K. Huang, S.-J. Liu, X. Y. Zhang, and Q. H. Liu, "A reconfigurable patch antenna with linear and circular polarizations based on double-ring-slot feeding structure," *IEEE Trans. Antennas Propag.*, vol. 70, no. 12, pp. 11389–11400, Dec. 2022.
- [8] H. Bahrami, S. A. Mirbozorgi, L. A. Rusch, and B. Gosselin, "Biological channel modeling and implantable UWB antenna design for neural recording systems," *IEEE Trans. Biomed. Eng.*, vol. 62, no. 1, pp. 88–98, Jan. 2015.
- [9] D. O. Rodriguez-Duarte, J. A. T. Vasquez, R. Scapaticci, L. Crocco, and F. Vipiana, "Brick-shaped antenna module for microwave brain imaging systems," *IEEE Antennas Wireless Propag. Lett.*, vol. 19, no. 12, pp. 2057–2061, Dec. 2020.
- [10] J. Blauert and A. Kiourti, "Bio-matched horn: A novel 1–9 GHz on-body antenna for low-loss biomedical telemetry with implants," *IEEE Trans. Antennas Propag.*, vol. 67, no. 8, pp. 5054–5062, Aug. 2019.
- [11] H. Wong, W. Lin, L. Huitema, and E. Arnaud, "Multi-polarization reconfigurable antenna for wireless biomedical system," *IEEE Trans. Biomed. Circuits Syst.*, vol. 11, no. 3, pp. 652–660, Jun. 2017.
- [12] T. Shaw, G. Samanta, and D. Mitra, "Efficient wireless power transfer system for implantable medical devices using circular polarized antennas," *IEEE Trans. Antennas Propag.*, vol. 69, no. 7, pp. 4109–4122, Jul. 2021.
- [13] K. Zhang, P. J. Soh, and S. Yan, "Design of a compact dual-band textile antenna based on metasurface," *IEEE Trans. Biomed. Circuits Syst.*, vol. 16, no. 2, pp. 211–221, Apr. 2022.
- [14] K. Zhang, P. J. Soh, and S. Yan, "Meta-wearable antennas-a review of metamaterial based antennas in wireless body area networks," *Materials*, vol. 14, no. 1, pp. 1–20, Jan. 2021.
- [15] K. S. Sultan, H. H. Abdallah, E. A. Abdallah, and H. S. El-Hennawy, "Metasurface-based dual polarized MIMO antenna for 5G smartphones using CMA," *IEEE Access*, vol. 8, pp. 37250–37264, 2020.
- [16] S. Yan and G. A. E. Vandebosch, "Radiation pattern-reconfigurable wearable antenna based on metamaterial structure," *IEEE Antennas Wireless Propag. Lett.*, vol. 15, pp. 1715–1718, 2016.
- [17] R. Joshi et al., "Dual-band, dual-sense textile antenna with AMC backing for localization using GPS and WBAN/WLAN," *IEEE Access*, vol. 8, pp. 89468–89478, 2020.
- [18] Y. B. Chauouche, M. Nedil, I. B. Mabrouk, and O. M. Ramahi, "A wearable circularly polarized antenna backed by AMC reflector for WBAN communications," *IEEE Access*, vol. 10, pp. 12838–12852, 2022.
- [19] A. B. Dey, S. Kumar, W. Arif, and J. Anguera, "Elastomeric textile substrates to design a compact, low-profile AMC-based antenna for medical and IoT applications," *IEEE Internet Things J.*, vol. 10, no. 6, pp. 4952–4969, Mar. 2023.
- [20] U. Purevdorj, R. Kuse, and T. Fukusako, "Broadband circularly polarized microstrip patch antenna with diamond-shaped artificial ground structure," *IEEE Open J. Antennas Propag.*, vol. 3, pp. 304–313, 2022.
- [21] H.-X. Xu, G.-M. Wang, J.-G. Liang, M. Q. Qi, and X. Gao, "Compact circularly polarized antennas combining meta-surfaces and strong space-filling meta-resonators," *IEEE Trans. Antennas Propag.*, vol. 61, no. 7, pp. 3442–3450, Jul. 2013.
- [22] K. Zhang, G. A. E. Vandebosch, and S. Yan, "A novel design approach for compact wearable antennas based on metasurfaces," *IEEE Trans. Biomed. Circuits Syst.*, vol. 14, no. 4, pp. 918–927, Aug. 2020.
- [23] R. B. V. B. Simorangkir, A. Kiourti, and K. P. Esselle, "UWB wearable antenna with a full ground plane based on PDMS-embedded conductive fabric," *IEEE Antennas Wireless Propag. Lett.*, vol. 17, no. 3, pp. 493–496, Mar. 2018.
- [24] R. B. V. B. Simorangkir, Y. Yang, L. Matekovits, and K. P. Esselle, "Dual-band dual-mode textile antenna on PDMS substrate for body-centric communications," *IEEE Antennas Wireless Propag. Lett.*, vol. 16, pp. 677–680, 2017.
- [25] R. B. V. B. Simorangkir, Y. Yang, K. P. Esselle, and B. A. Zeb, "A method to realize robust flexible electronically tunable antennas using polymer-embedded conductive fabric," *IEEE Trans. Antennas Propag.*, vol. 66, no. 1, pp. 50–58, Jan. 2018.
- [26] S. Di Meo et al., "Tissue-mimicking materials for breast phantoms up to 50 GHz," *Phys. Med. Biol.*, vol. 64, no. 5, Feb. 2019, Art. no. 055006.
- [27] SPEAG, "DAK—Dielectric assessment kit," 2023. [Online]. Available: <https://speag.swiss/products/dak/overview/>
- [28] J. Shang and Y. Yu, "An ultrawideband capsule antenna for biomedical applications," *IEEE Antennas Wireless Propag. Lett.*, vol. 18, no. 12, pp. 2548–2551, Dec. 2019.